ICP-CVD μ-Si Layers Optimization for Strain Gauges on Flexible Substrates

F. Garcia Castro, O. de Sagazan, N Coulon, C. Simon, F. Le Bihan

*Fatima Garcia Castro****: Investigation***
*Olivier de Sagazan****: Conceptualization, Methodology, Writing - Original Draft, Investigation***,
*Nathalie Coulon: **Writing - Review & Editing***, ***Supervision***
*Claude Simon: **Investigation***
*France Le Bihan: **Writing - Review & Editing***, ***Supervision, Project administration***

ICP-CVD µ-Si Layers Optimization for Strain Gauges on Flexible Substrates

Fatima Garcia Castro, Olivier de Sagazan, Nathalie Coulon, Claude Simon, France Le Bihan

Univ Rennes, CNRS, IETR, UMR 6164, F-35000 Rennes, France

Corresponding author: O de Sagazan
Olivier.de-sagazan@univ-rennes1.fr 0033 2 23 23 52 67

Abstract

Low Temperature µ-Si layers were performed in a Corial Inductively Coupled Plasma Chemical Vapour Deposition (ICP-CVD) system. Doped µ-Si layers have been investigated in terms of resistivity, contact resistance, crystalline fraction and Gauge Factor. Some parameters have been identified to increase the Gauge Factor (GF) or the crystalline fraction (Fc). Strain gauges performed on 25 µm thick polyimide (PI) film have been tested to show the interest of the ICP-CVD µ-Si technology in the field of pressure sensors.

Author Keywords

ICP-CVD; PECVD; Strain Gauges; TLM; µ-Si doped; flexible electronics; low temperature electronics, strain gauges fabrication.

1. Introduction

Flexible electronics is today a major research field due to a fast growing market. Numerous devices on flexible substrates are under development with high promising prospects in robotics [1], health monitoring [2], epidermal electronics [3], intelligent textiles [4] or photovoltaics. Most resistive strain sensors are limited when it comes to monitoring high deformations induced by small bending radius in range of few millimetres or when high spatial resolution is required. Therefore, the aim of this work is to develop sensors on flexible substrates able to measure such local deformations.

Two main types of materials are used as strain gauges: metals and semiconductors. Other materials such as organic semi-conductors [5], graphite [6], carbon nanotubes [7] or conductive polymer composites [8] are discussed in the literature but are not still matured. The gauge factor (*GF*) is typically used to quantify the sensitivity of a resistive strain sensor and is defined by **Eq. (1)** as the ratio between the relative change in its electrical resistance ($\Delta R/R_0$) and the strain ε applied to that sensor:

$$GF = \frac{\Delta R/R_0}{\varepsilon} \qquad (1)$$

For metal gauges, the GF is low, between 2 and 5 [9]. Their low resistivity also implies a large active area, which severely limits the achievement of accurate spatial resolution. For semiconductors, especially silicon-based materials, the GF has much higher values due to the so-called piezoresistivity effect resulting from crystal lattice deformation, i.e. about 100 for single-crystal silicon (sc-Si). In the case of disordered silicon layers with grains and grain boundaries, the gauge factor is lower [10], i.e. 20-40 for polycrystalline silicon (poly-Si) [11] or 20-30 for amorphous silicon (a-Si) [12]. In this case, the piezoresistivity related to the value of the gauge factor is difficult to model because it depends on the grains size, their orientation and their doping, the contribution of the grain boundaries, ... Overall, the gauge factor of these materials increases when the doping, beyond a certain threshold, decreases [10-13]. These materials also have other advantages such as the possibility of being deposited on various substrates as well as flexible or the adjustment of their resistivity by doping, allowing the design of measurable resistances in limited spaces

Silicon films can be deposited in an amorphous or crystallized phase by plasma enhanced chemical vapor deposition (PECVD) at low temperature (< 250 °C). Microcrystalline silicon (µ-Si) with grain size around 20nm and a crystalline fraction over 50% is more stable and can lead to higher electrical performances. Usually µ-Si:H (hydrogenated µ-Si) or nc-Si:H (hydrogenated nanocrystalline silicon) thin films are deposited at low temperature ($T \sim 250$–300 °C) by PECVD with silane highly diluted in hydrogen [14]. At lower deposition temperature, around 150 °C, µ-Si:H films are stressed and generally more or less porous [15], the electrical mobility obtained remains low with respect to the potential applications. A better quality of µ-Si:H or nc-Si:H deposited at low temperature could be achieved by PECVD by diluting H_2, Ar and SiH_4 [16]. Indeed, in the past, some research has been carried out to investigate the effect of Ar dilution on the deposition of amorphous and microcrystalline silicon by PECVD. Some interesting results have been obtained in this way, leading to the production of TFTs (Thin Film Transistors) using µ-Si elaborated below 200°C by PECVD [17].

Strain gauge using a µ-Si film deposited directly as a piezoresistive material on a 50 µm thick polyimide (PI) substrate, were performed by PECVD in H_2/Ar dilution and investigated [18]. Those strain gauges were individually studied with tensile and compressive bending tests with a wide range of variation (up to 5 mm bending radii) by the Transmission Line Method (TLM) to directly extrapolate the resistivity of the µ-Si film and the associated GF [18]. According to the knowledge acquired on µ-Si strain gauges processed by PECVD, it was decided in the present work to explore the electrical, physical and mechanical properties of ICP-CVD µ-Si:H layers. In this paper, an ICP-CVD reactor has been used to perform µ-Si doped thin layers on 25µm PI sheets. TLM structures have then been performed on these layers to extract Gauge Factor, sheet and contact resistance and resistivity.

In this work, an ICP-CVD machine will be briefly presented with its advantages and the various deposit modes it can provide, such as RF bias adjunction or pulsed mode either on RF or ICP power. Then, different parameters have been investigated to study their impact on the resistivity of µ-Si layers, the crystalline fraction and the gauge factor.

2. ICP-CVD presentation, reactor description and gas facilities

The use of Inductively Coupled Plasma Chemical Vapour Deposition (ICP-CVD) for performing Si layers at low temperature appears to be very interesting and several works report this method. Some TFTs have been fabricated using ICP-

CVD for the deposition of active semiconductors or insulators. This method has been widely used for the application of a-Si targeting solar cell [19-20-21] and especially to create a-Si/µ-Si heterojunctions [22] to improve the efficiency of solar cells. ICP-CVD is also used for SiC deposition [23], finding application in Micro Electro Mechanical Systems MEMS fields [24]. ICP-CVD doped layers have been reported [25], but with boron and for solar cell application. In this case, it leads to quite high resistivity value even with N type dopant such as phosphorous [26], all these works report the dilution of AsH_3 and PH_3 in H_2 and SiH_4 only. The use of H_2 dilution has already been investigated [27] but it does not seem that SiH_4+Ar+H_2 mixture has been used for µ-Si and especially for the realization of the TLM in the ICP-CVD process as we propose in the following study.

General description: The Corial 210D ICP-CVD machine (Figure 1) is a reactor using pure SiH_4 combined with carrier gasses such as H_2 or Ar. It is possible to add PH_3, AsH_3 and B_2H_6 for in-situ doping. For the insulator process, it is also possible to add in plasma N_2 or NH_3 for nitride deposition, or O_2 or N_2O directly for oxide deposition. A CF_4 line gas is also available to clean the reactor chamber by CF_4/O_2 plasma. The machine has two generators, one dedicated to RF plasma, and the other for ICP power, which could reach 1000 W. Both generators can be controlled in pulsing mode. The pumping system is able to achieve the process at 2 mTorr (depending on carrier gas flow level) and 2 to 6 inches substrates can be processed.

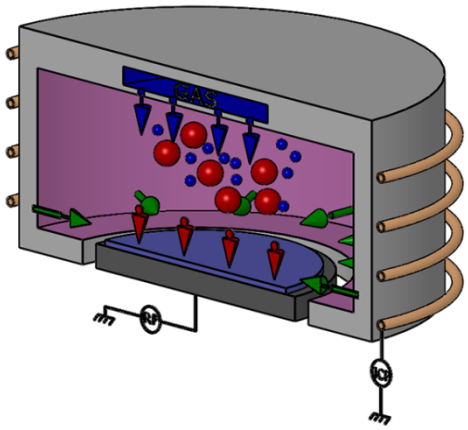

Figure 1. Corial ICP-CVD reactor cross section, showing anode and cathode with antennas around. The carrier gas inlet (blue) from the anode's holes and reactant gas inlet coming from the side walls (green).

Thermal monitoring: During processing, the substrates are thermally controlled with a He flow, which ensures thermal conduction with the cathode. The cathode temperature can be monitored from 5 °C to 150 °C, and substrates could even reach 200 °C by using a special substrate holder. The main interest of ICP-CVD plasma is to produce a high density plasma, where the dissociation rate is very high. Hence, it becomes possible to carry out chemical reactions at low temperature and low pressure with a good deposition rate. Moreover, the absence of RF power prevents the bombardment effect induced by the voltage bias, which could lead to voids inside the layers. Another interesting aspect of the ICP-CVD reactor comes from the generally low temperature for all kinds of processes. Indeed, low temperature widely decreases risks of cross contamination, and thus allows the deposition of monolayers (undoped / doped) as well as layers of different natures in the same reactor (oxide, nitride, µ-Si, a-Si). In our case, it appears that below 150°C no doping is effective. That's the reason why the special substrate holder was used to reach temperature between 150°C to 200°C, keeping the LTPS (Low Temperature Poly-Silicon) range of Si.

This special substrate holder is a quartz shuttle which deliberately degrades the thermal contact between the cathode and the substrates. By this way it becomes possible to reach higher temperature due to the self-heating effect of ICP plasma. The temperature is then monitored by performing a first N_2 plasma during 5 min before deposition to reach a thermal stability. In this case, the temperature level is defined by the power of this first N_2 ICP plasma (figure. 2).

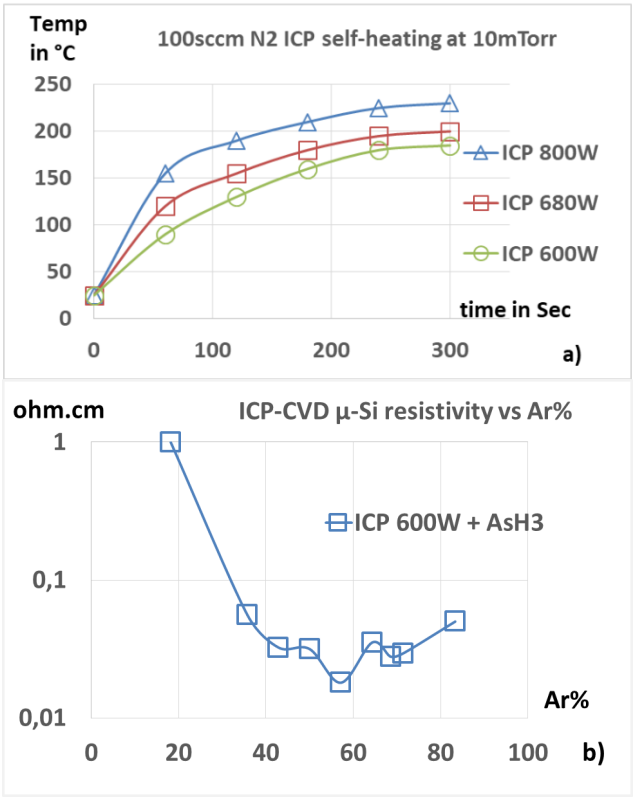

Figure 2. a) Thermal calibration for special substrate holder using 100sccm N_2 ICP at 10mTorr. b) Impact of Ar dilution in the ICP-CVD mixture ($SiH_4/H_2/Ar/AsH_3$) on µ-Si resistivity at 4mTorr Deposition is achieved on oxidized wafer.

Dopant gases and precursor: For the following experiments, the dopant gases used were diluted in H_2 at 0.1%, either for PH_3 or AsH_3. In next graphs, the dopant flow rate expressed in sccm (Standard Centimetre Cube per Minutes) corresponds to the diluted flow. The precursor gas used in all experiments is pure SiH_4.

Deposition process: Before all deposition, a N_2 plasma step (5 min 100 sccm at 10mTorr and 600W) is achieved to reach 185°C at the PI surface. The deposition step is then launched by adjusting pressure and ICP power just before sending SiH_4 and dopant in a H_2/Ar mixture regulated at 4mTorr. Deposition rate settles around 10 to 20 nm/min in case of µ-Si doped layers. Effects of Ar adjunction in PECVD have been investigated previously [17] and its positive impact has been demonstrated on Fc as well as on doping efficiently. In short preliminary test influence of Ar % in the gas mixture has also been investigated in

the case of ICP-CVD µ-Si films (Figure 2b). These tests performed on oxidized wafers present lower resistivity that those obtained on flexible films but variations are identical. It appears that with a fixed SiH_4/AsH_3 ratio the resistivity depends widely on the percentage of Ar in the gas mixture with minimal resistivity reached around 55% of Ar in the mixture. It demonstrates the positive impact of Ar on ICP-CVD µ-Si layers as previously noticed in PECVD even if the range of power and deposition pressure are totally different, around 1Torr in PECVD and several mTorr in ICP-CVD.

3. Crystalline Fraction and Gauge Factor measurement.

Several experiments have been driven to determine effects of ICP-CVD parameters on the crystalline fraction and gauge factor GF.

Crystalline Fraction: To determine the crystalline fraction (Fc), µ-Si layers have been deposited on glass substrates and the material has been analysed by Raman spectroscopy to determine its Fc [28]. The µ-Si films contain crystalline zones separated by grain boundaries (amorphous zone). By using Raman spectrometry, it is possible to determine the crystallization level also called the crystalline fraction ($Fc_{\%}$).

The spectrum gives us more information about the chemical bonds between radicals. The spectrum is formed by the convolution of 3 Gaussian contributions as shown in figure 3.

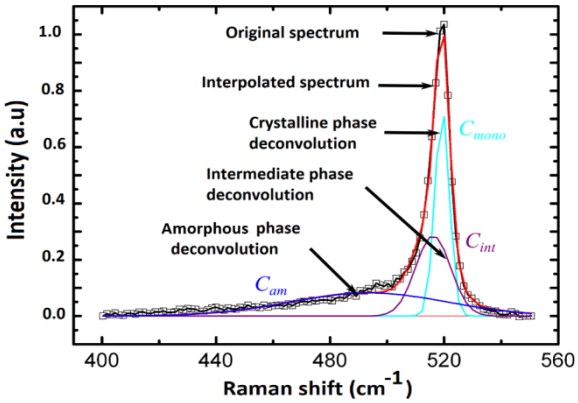

Figure 3. Raman spectrum deconvolution for three curves.

The amorphous phase of silicon (C_{am}) corresponds to the integral of Raman intensity centered at 480 cm^{-1}.There is an intermediate phase (C_{int}) that corresponds to a defective crystalline phase, with a center around 510 cm^{-1}. It highlights the presence of grain boundaries and crystallites with dimensions smaller than ten nanometers [29].

The crystalline phase of silicon (C_{mono}), shown as a narrow Gaussian curve centered at 520 cm^{-1}, corresponds to the crystalline phase of the material. The position and width of the Gaussian depend on grain size and stresses in the material. [30-31-32].

Once this deconvolution has been achieved, the calculation of the area under each curve allows to determine the crystalline fraction using the formula 1.

$$Fc\% = \frac{C_{mono} + C_{int}}{C_{mono} + C_{int} + C_{am}} \qquad (1)$$

Gauge Factor Measurement:

The structure is based on a Transmission Line Method (TLM). The aim here is to measure the resistivity ρ of a semi-conductor film and the contact resistance R_C at the semi-conductor/metallic contact interface. Indeed, considering R_T as the total resistance measured (see figure 4):

$$R_T = \rho L/(dW) + 2R_C + R_{routing} \quad (2)$$

where ρ is the resistivity of the semi-conductor (µ-Si here) and L, W and d, are respectively length, width and thickness of the semi-conductor resistor. The resistance of the metallic routing $R_{routing}$, aluminum (Al) here, can be neglected since $R_{Al} << R_{\mu Si}$. Then the plot of R_T as a function of L leads to a straight fit (if contacts are ohmic) with a slope proportional to the resistivity ρ and the intersection of the fit with the R-axis gives information on R_C.

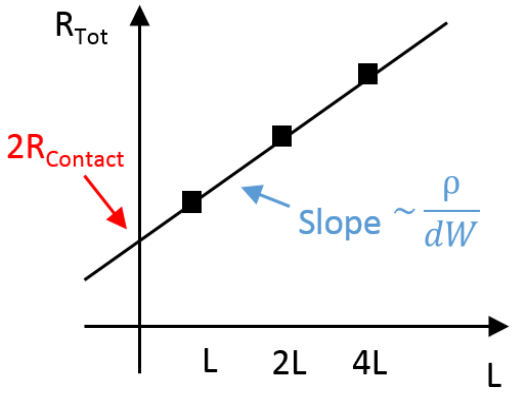

Figure 4. Graphic used to extract TLM parameters [33].

In our case, the purpose is to measure the resistivity for several radii of curvature to quantify the sensitivity of the µ-Si film as a strain sensor. As stated previously using the general equation for a resistance $R = \rho L/(dW)$, we can then obtain $\Delta R/R = \Delta\rho/\rho + \Delta L/L(1+2\nu)$, where ν is the Poisson's ratio of the resistor material. The second term $\Delta L/L(1+2\nu)$ denotes the geometrical effect during bending. The first term $\Delta\rho/\rho$ is the relative resistivity variation and denotes the piezoresistive effect. For a poly-Si material, it is define as follows:

$$\Delta\rho/\rho = \pi_L\sigma_L + \pi_T\sigma_T,$$

where π_L, π_T are the longitudinal and transversal piezoresistive coefficients of poly-Si respectively and σ_L, σ_T are the applied longitudinal and transversal stresses respectively. Thus, being able to extract resistivity ρ makes it possible to directly study the resistivity variation $\Delta\rho/\rho$ for each radius and this gives direct information on the piezoresistive coefficients. In this study, we focused on the longitudinal sensitivity.

TLM fabrication process:

The fabrication process starts by a cleaning step of a 10x10 cm² large and 25 µm thick PI substrate with acetone, alcohol and deionized water. The active layer, a 100 nm thick doped µ-Si film, is deposited using various conditions and islands-like are patterned by Reactive Ion Etching (RIE) using a SF_6 plasma. A 300 nm thick aluminum layer (Al) is deposited by thermal evaporation and patterned by wet etching to form electrodes and test pads (figure 5). The sample is subjected to a final thermal annealing at 180°C for 2h, this last step improves the general µ-Si

resistivity as well ohmic contact between Al and µ-Si.

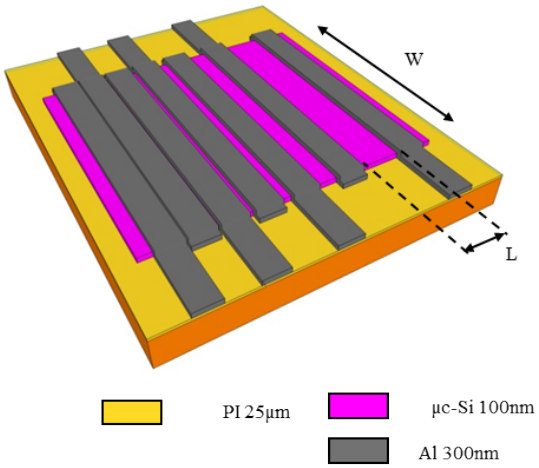

Figure 5. Schematic of a final TLM structure. Each structure is composed of 6 resistors, corresponding to 6 lengths *L* (5, 10, 20, 40, 80 and 160 µm). 4 different widths *W* are also studied (1000, 500, 250 and 125 µm), which results in 24 different resistors.

In order to quantify the piezoresistive effect, strain gauges are measured when the substrate is bent with different radii of curvature *r*. Several methods are commonly used and can be separated in 2 categories: dynamic and static bending tests. Dynamic measurements may provide more informative results but require sophisticated instruments such as homemade ones or 4-point bending tests [34]. Moreover the 4-points method, which is very common in the silicon industry, does not allow high bending. Static tools are easier to handle but measurements can be difficult when using flexible substrates and low radii of curvature ($r \leq 5$ mm). In our bending test bench [18], a 2-wire static I-V method is used. 4 TLM structures are measured for each radius, resulting in 4 resistances These 4 cells are placed on the same bending axis. Figure 6 shows the homemade tools used for the tensile stress tests. According to the samples, 4 tensile radii of curvature (2.5, 2, 1.5, 1cm) were used.

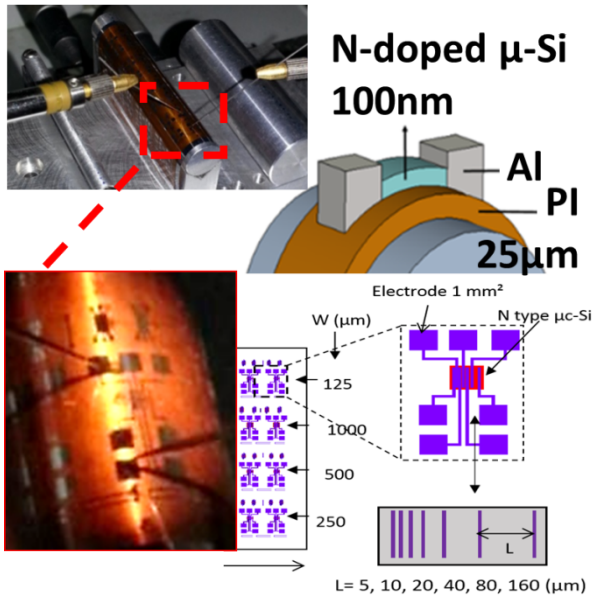

Figure 6. Homemade tools (steel cylinders) used for static I-V measurements under bending for tensile tests and scale of the patterned TLM device.

I-V measurements are performed with an Agilent B1500A at room temperature (regulated 20°C), with an applied voltage between ± 1 V. For the calculated resistances, values at + 1 V are taken into account. The procedure consists in a first measurement without bending (flat substrate) to obtain the initial value. The sample is then fixed on the tensile bending tools from the lowest curvature (i.e. highest radii) to the highest curvature (i.e. lowest radii). Between each bending, the resistors are measured and then re-flattened to evaluate the reliability. The study is focused on the longitudinal *GF*, so the length *L* of the resistors is perpendicular to the bending axis i.e. the current flow is parallel to the curvature direction.

Strain Calculation:

For each radius of curvature, the strain applied to the structure is calculated using a bi-layer model as a function of their Young's modulus value *Y* [35], (Figure 7). In our case, the material properties are presented in Table 1. The Al electrodes are not represented since we focus on the channel of the resistor, between the 2 contacts. The bi-layer model is thus constituted by the PI substrate and the µ-Si layer.

Layer	PI	µ-Si
Thickness	25 µm	100 nm
Y (GPa)	2.5 [36]	80 [37]

Table 1. Material properties used in this paper.

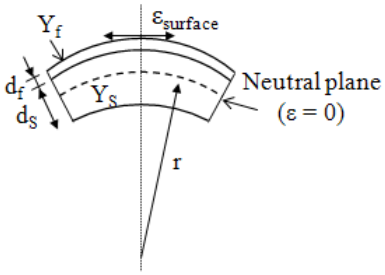

Figure 7. Schematic cross-section of the mechanical model. The names refer to **Eq. (2)**.

The longitudinal strain $\varepsilon_{surface}$ on the surface of the top layer is given by the equation derived from [37]:

$$\varepsilon_{surface} = \left(\frac{d_f + d_s}{2r} \right) \frac{\left(1 + 2\chi\eta + \chi\eta^2\right)}{(1+\eta)(1+\chi\eta)} \text{ Where}$$

$$\eta = \frac{d_f}{d_s} \text{ and } \chi = \frac{Y_f}{Y_s} \quad (2)$$

With *r* the applied radii of curvature, d_S and d_f respectively the substrate and the layer thicknesses, and χ and η defined by

$\chi = Y_f/Y_S$ and $\eta = d_f/d_S$, where Y_S and Y_f are substrate and layer Young's modulus respectively. The plus (or minus) sign depends on the bending applied opposite to (or with) the built-in curvature.

The table 2 shows the different values of strain applied to the 25µm thick Kapton (PI) and µ-Si TLMs for each radius of curvature.

Radii curvature	Top surface strain calculation ($\varepsilon_{surface\ \%}$)
	Kapton® (25 µm) + µC-Si (100 nm)
R = 2.5cm	0.045
R = 2cm	0.056
R = 1.5cm	0.074
R = 1cm	0.112

Table 2. Top surface strain according to radii of curvature.

This method using a cylindrical bending test bench was previously used to determine the influence of mechanical stress in µ-Si thin film transistor (TFT) [38] and was then adapted to determine the GF of µ-Si layers issue from PECVD for strain gauges development. The PECVD µ-Si layers were then investigated, showing GF=-28 in the tensile domain and -37 in the compressive domain [18]. In order to further validate our test bench with a 25 µm thick substrate, TLMs were performed using the already known AsH_3 doped µ-Si PECVD layers [17].

These TLMs on a 25 µm PI substrate present a GF = -27 in the tensile domain as shown in figure 8. This GF, similar to the one measured previously, allows us to validate the coherence of our experimental setting. This value is similar with previous works on nc-Si:H thin layers measuring GF around -30 in case of N-type films obtained by HW-CVD and PECVD [34-39-40].

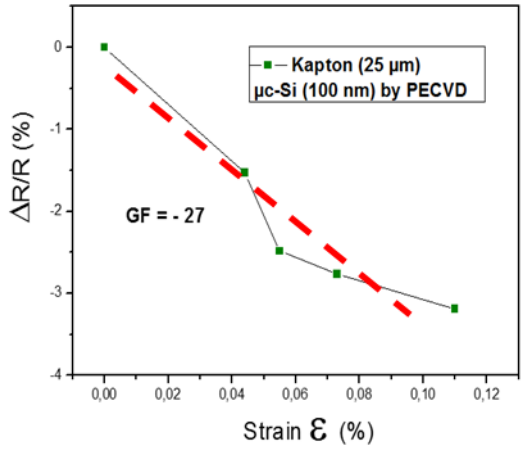

Figure 8. As doped µ-Si layers Gauge factor determination by deformation of the TLM structure on a bending test bench (100nm µ-Si layers on 25µm Kapton). Red line shows the graphical method used to extract GF.

4. Effect of ICP- CVD parameters on µ-Si characteristics.

Several experiments were carried out, each time a 100 nm thick layer of µ-Si was deposited and then processed to perform a TLM structure.

In the following experiments (table 3), the nature of dopant, its concentration and the influence of RF power have been investigated. The ability to apply pulses was also especially tested to see their impact. In the case of RF pulses, every 4 seconds a 40W pulse is applied during 400ms. In case of ICP pulses, a 900W pulse is applied during 400ms every 4 seconds keeping a base power at 600W.

ICP Power in W	RF Power in W	dopant/Si	Si partial pressure in mtorr	dopant in sccm
600	0	1,000E-02	1,111E-01	20PH3
600 / 900pulsed	0	1,000E-02	1,111E-01	20PH3
600	40 continious	1,000E-02	1,111E-01	20PH3
600	40 puls	1,000E-02	1,111E-01	20PH3
600	40 puls	1,000E-02	1,111E-01	20 AsH3
600	0	1,000E-02	1,111E-01	20 AsH3
600	0	2,500E-03	1,404E-01	5 PH3
600	0	5,000E-03	1,290E-01	10 PH3
600	40 puls	5,000E-03	1,290E-01	10 PH3
600	40 puls	5,000E-03	1,290E-01	10 AsH3

Table 3. ICP-CVD conditions for TLM µ-Si layers

Each structure has been tested on the bending measurement system. According to the different radii of curvature, resistance shifts have been plotted as a function of the applied deformation strain. The calculated slope defines for each ICP-CVD conditions a dedicated GF and ρ. For all conditions, several TLM structures were performed and stressed on the bending test bench with 4 cylinders of different radii, thus applying 4 different stresses. The figure 9 shows the calculation of the GF for 4 different deposition conditions. The slopes have been extracted for each deposition condition using several different TLMs (allowing boxplots generation) from the graph of the shift resistance versus elongation strain. Some wide variations have been obtained but still in the general range of GF measured in case of PECVD nc-Si:H films [39-40]. This distribution of GF highlights the strong impact of ICP-CVD parameters on low temperature Si film characteristics.

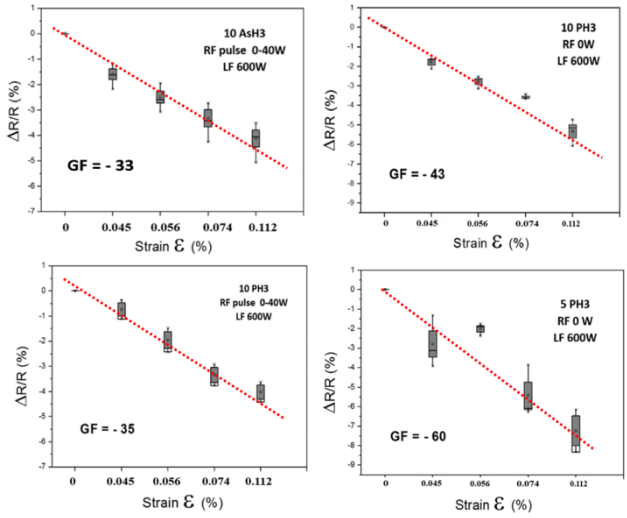

Figure 9. Determination of ICP-CVD µ-Si layers Gauge Factor by extraction of the slope ΔR/R = f(ε) for 4 different µ-Si deposit conditions.

TLM parameters extraction and basic links: In a first analysis, the relationship between resistivity and GF has been plotted in figure 10a. As expected [11-13], in this range of carrier concentration (above $1.10^{19}cm^{-3}$ measured by Hall effect), there is a general trend that leads to an increase in the GF (in absolute value) when resistivity increases. However, since the linearity of the regression is quite low, it shows that other parameters should be taken into account to explain the variation in the GF. TLM (Figure 4) allows also to extract contact resistance (Rc) and the

sheet resistance Rsh [41]. In fact, it consist on plotting the slope of TLM characterization (3) taking in account the width of TLM device in present case W=1000µm.

$$R_{sh} = \frac{\Delta R}{\Delta L} W \quad \text{with W= 1000µm} \quad (3)$$

The ratio Rc/Rsh has been calculated and plotted on figure 10b, it shows a direct relationship with GF at low value of ratio. It seems that under a certain value of Rc, (200 Ohm) increase of GF is directly related to a decrease of Rc. For higher value of Rc in case of 10sccm of AsH_3 under RF pulse and 5sccm PH_3 condition, respectively Rc 350 Ohm and 1700 Ohm other parameters should predominate.

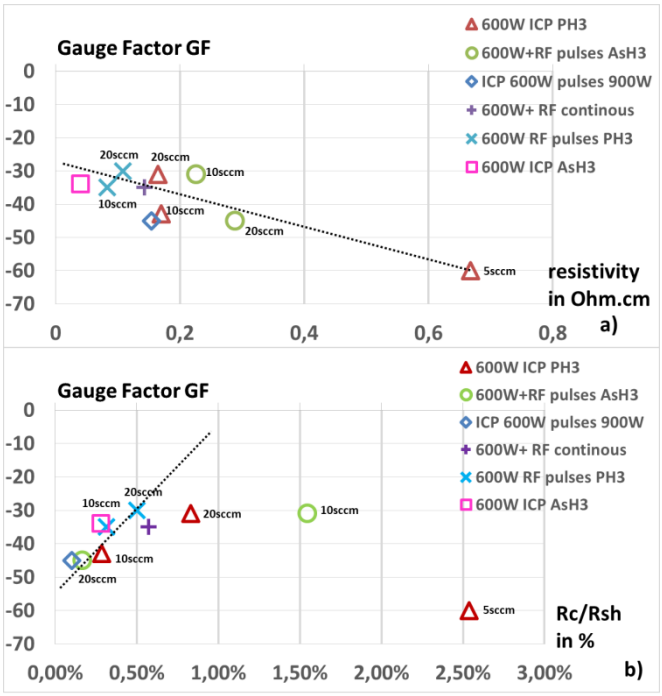

Figure 10. a) Correlation between GF and resistivity independently of ICP-CVD conditions. b) GF according Rc/Rsh for different deposition conditions.

In fact, piezoresistive coefficients could depend on several parameters (doping level, nature of dopant, grain size, crystalline fraction, which have been studied especially for c-Si and poly-Si [11] and also experimented [13]. Data and experiments are more limited in case of low temperature Si layers such as µ-Si. Through these TLM tests, the general relationship between resistivity and GF appears, as well as an impact of the contact resistance Rc on the GF value. This work aim to investigate more deeply the impact of different deposition parameters such nature/concentration of dopant or plasma functioning mode on the final piezoresistive layer characteristics.

Resistivity: The resistivity of µ-Si layers used for TLM shows a quite wide variation according to the deposition conditions. Figure 11 first shows, as expected, the link between dopant flow and resistivity, with a maximum resistivity obtained for a PH_3 flow of 5sccm. But it also reveals that the dopant is mainly in overflow and that 10sccm of PH_3 should be enough to reach the minimum resistivity available.

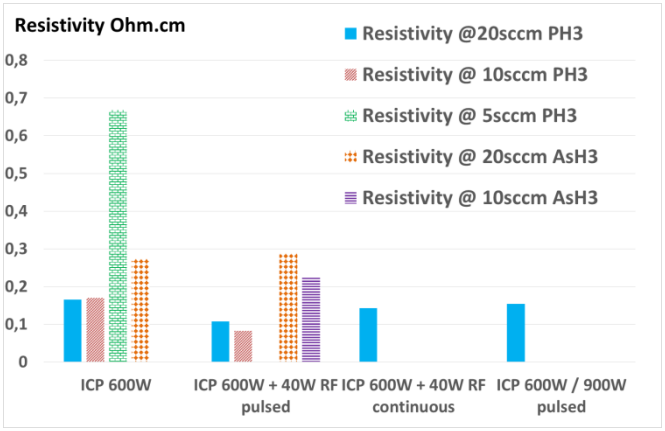

Figure 11. Resistivity determined by TLM at the rest position for different ICP-CVD conditions.

The nature of dopant also plays a role, with AsH_3 leading to a quite higher resistivity compare to PH_3. The impact of the different generator functioning modes on resistivity is not obvious, only the RF pulsed mode appears to be efficient to increase the incorporation of P and moreover at medium PH_3 concentration. In case of As, some effect of RF pulses were noticed but only at low As concentration, it could also be due to the overflow of AsH_3. The pulsed mode on ICP power and the continuous RF power, hardly do not affect the final resistivity of the layer.

Gauge factor: Regarding the gauge factor, some significant changes have been measured according to the deposition mode, as shown in Figure 12.

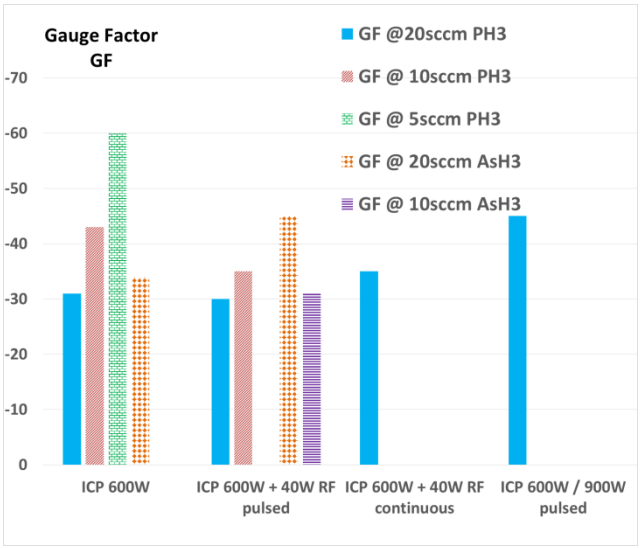

Figure 12. GF according to different ICP-CVD conditions.

The maximum GF is obtained as expected with a low PH_3 concentration which was also the highest resistivity result. The 900W ICP pulses widely improve the GF compared to other 20sccm PH_3 conditions. A medium PH_3 concentration also provides a good GF with single ICP power, this one is slightly lowered when adding RF pulses. Some variations are interesting to note. In case of a high PH_3 concentration (20sccm), the pulsed RF does not affect the GF, unlike the ICP pulsed mode, whereas in case of high AsH_3 concentration, the effect is very significant. Continuous RF slightly improves the GF under conditions of high

concentrated PH_3 conditions.

The best GF results are obtained at low and medium PH_3 concentration at 600W of single ICP power, when adding ICP 900W pulses and also at high concentration of AsH_3 in the RF pulsed mode. In fact, since GF and resistivity are linked so it is necessary to separate the effect on GF induced by low resistivity from the other effects induced by deposition parameters.

Moreover, for some applications, a lower resistivity will be a crucial advantage in terms of frequency response or induced parasitic resistance. In order to highlight the variation of GF independently of resistivity shifts, a normalized ratio has been defined with a reference value for crystalline silicon with a GF=100 and a resistivity at 0.1 Ohm.cm (formula 4), the variation of this parameter is shown in figure 13.

$$normalized\,ratio = \frac{Gf}{\rho} * \frac{0.1}{100} \quad (4)$$

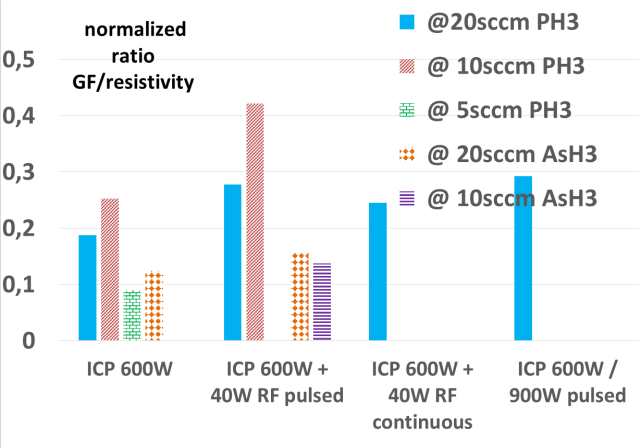

Figure 13. Normalized ratio GF/resistivity according to different ICP-CVD conditions. This coefficient highlights the contribution of deposition, condition regardless of the resistivity level.

This presentation reveals the efficiency of the pulsed mode on a medium PH_3 concentration, combining a low resistivity with a slightly higher GF. The efficiency of ICP pulses is also validated by this mode of presentation combining a high GF and a low resistivity as well. The previous high GF result attributed to the AsH_3 (20sccm) in RF pulsed mode is now moderated by this presentation. For PH_3 the best dilution of dopant should be between 10 to 20sccm for maximizing GF at the lowest resistivity. The RF pulse mode has a positive impact for PH_3, but only at high concentration in case of AsH_3.

Crystalline Fraction: In order to understand which factor leads to a higher GF or how the dopant (level / nature) interacts with the deposition mode, the crystalline fraction (Fc) of some deposits have been investigated by Raman spectroscopy on glass substrates. It was shown previously that Fc of µ-Si film deposited on glass or PI is the same. Results of Fc and GF are exposed on Figure 14a.

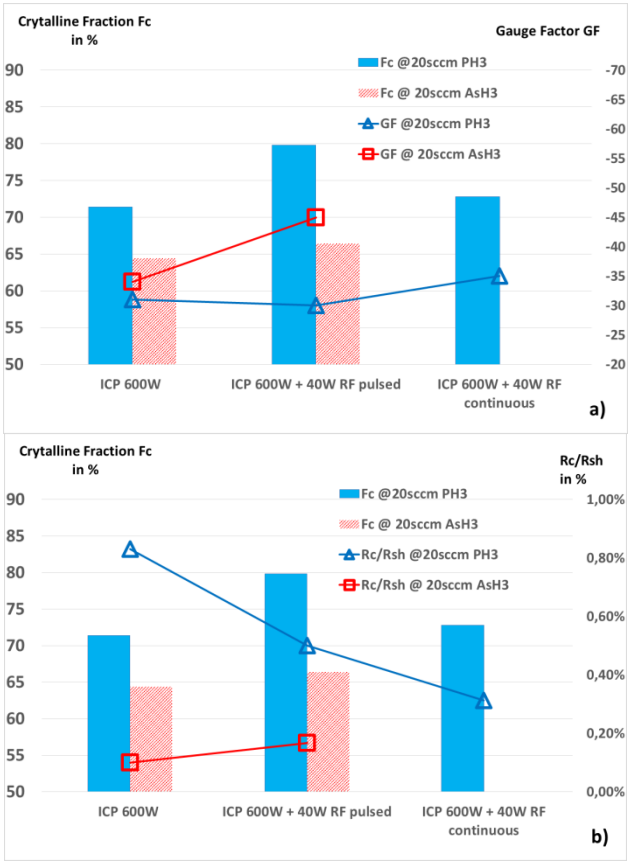

Figure 14. a) Evolution of Fc and GF for PH_3 and AsH_3 doping under various deposition conditions. b) Relationship between contact resistance ratio and Fc for different doping and deposition mode.

Results on Fc for high concentration of PH_3 show no direct relationship with GF, it seems that these two parameters are completely independent under these dopant concentration conditions. In fact, the highest GF measured corresponds to a medium Fc and the lowest GF to the highest Fc, anyway all these variations are weak and GF could be considered as constant. It appears that RF pulses widely increase the Fc in the case of PH_3. In case of AsH_3 doping, a small increase in Fc is brought by the RF pulse mode, which is linked with a high increase in GF. Results are similar in case of Rc/Rsh ratio, no direct relationship could be done between Fc and Rc/Rsh. It just appears clearly that RF adjunction decreases this parameter in case of P doping whereas it slightly increases for AsH_3 doping as it is shown in figure 14b.

Uniformity deposit:

A final parameter that could give some information on the deposition characteristics, is the relative standard deviation of resistivity. It is possible to define a kind of uniformity by expressing this relative standard deviation as a percentage (formula 5). This is shown in figure 15.

$$uniformity = \frac{Stdev(\rho) * 100}{\rho} \quad (5)$$

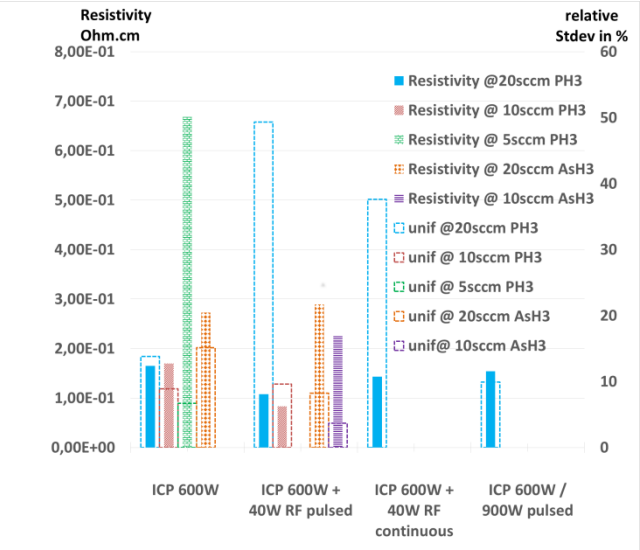

Figure 15. Uniformity of resistivity is defined as the percentage of the relative standard deviation from its resistivity value for each deposit condition.

This figure 15 shows the poor impact on uniformity induced by the combination of a high PH_3 concentration and RF pulsed mode or even continuous. On the contrary, in the case of AsH_3, RF pulses seem to improve this uniformity. The last interesting result is the positive influence of the ICP pulses on the uniformity.

Discussion and proposed model:

The main results from these experiments are listed here:

-The dopant flow and its nature is a key factor. At a low or medium PH_3 flow, GF and resistivity are inversely linked, which is the normal behavior of Si layers in this range of doping (1.10^{-19} cm^{-3} [11-13]). At a high PH_3 concentration, the saturated resistivity and GF are lower. Figure 16 summarizes the different factors acting on GF and proposes a model introducing a phosphorus trap density (P trap density). According to the proposed model, non-active P inside µ-Si layer defined as a P trap density, possibly located within the amorphous grain boundaries, negatively acts on the GF factor as also on Rc/Rsh ratio. Thus, when this P trap density decreases (according on the deposition mode), it induces an increase in the GF.

In case of As, the GF is quite similar with a higher resistivity. Here also, AsH_3 is in overflow, but in this case it degrades the As incorporation capability, leading to an unusual increase in resistivity with the AsH_3 flow. That's why the resistivity is lower at a medium AsH_3 flow.

-The ICP pulsed mode delivering a peak of 900W over a short period seems to be very promising for the improvement of the GF. Moreover, it also increases the uniformity of resistivity in case of highly concentrated PH_3 µ-Si layers, keeping also a low level of resistivity. Moreover this mode of deposition leads to a very low ratio Rc/Rsh (0.1%), this result is one of the best compromises. We can explain this by using the model in Figure 16 and conclude that the ICP pulsed mode acts mainly by decreasing the level of non-active P in the grain boundaries of layer, which considerably decreases this P trap density, thus allowing a substantial increase in GF.

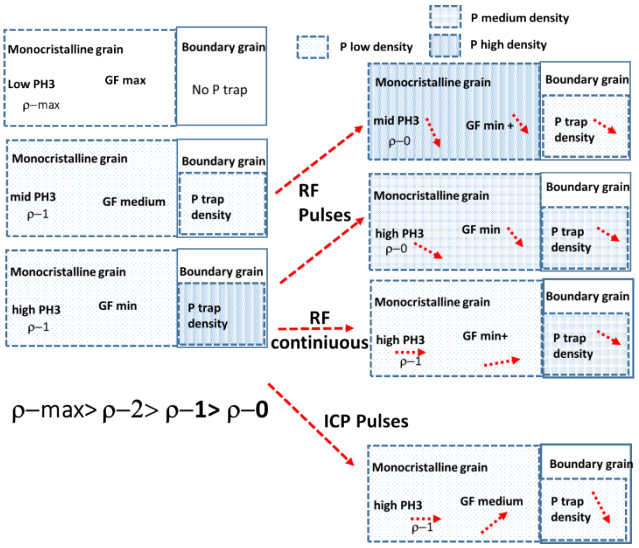

Figure 16. Summary of different effects induced by the ICP mode and the dopant flow in case of N-type layers. Model of the additional action of non-active phosphorus atoms on the GF as a trap density inside the amorphous phase. Arrows show impact on different parameters such Resistivity (ρ), GF or trap density.

- The RF pulse during deposition increases the Fc at a high concentration of PH_3, it induces a decrease of resistivity and contact resistance ratio as expected but no GF change. This steady GF in this case (or small decrease in medium PH_3) is due to the simultaneous decrease of P trap density which compensates the decrease in resistivity and thus maintains the GF level. Unfortunately, this deposition mode degrades the uniformity of the resistivity of the P layers, tempering its advantages.

In case of As, the RF pulses do not increase the Fc but strongly increase the GF without changing the resistivity, improvements are quite noticeable also in term of Rc/Rsh ratio. In this case, according to the proposed model, the As trap density is also decreased by the RF pulses, which lead to a strong increase of GF because it is not compensated this time by a resistivity decrease (figure 17). Unlikely to phosphorous the RF pulses on arsenic do not induce a degradation in resistivity uniformity.

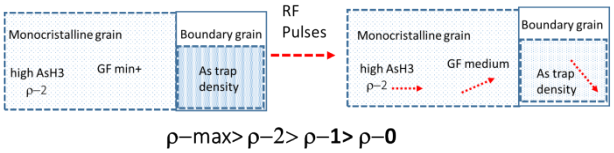

Figure 17. RF pulses effect on As doped layers and GF increases with the impact on As trap model.

- The continuous RF addition at high PH_3 concentration does not affect the resistivity or the Fc but slightly increases the GF as the RF pulses do and, probably by the same process, also decreases the uniformity of resistivity. It seems obvious that bias voltage purchase by the RF mode widely improves the ratio Rc/Rsh leading to a better general contact resistance.

The study of uniformity, i.e the relative standard deviation of resistivity expressed as a percentage, shows a degradation of uniformity in case of P with RF pulses and on the contrary an improvement in case of As or ICP pulse. This could again prove that both dopants do not behave in the same way when RF pulses

or ICP pulses are applied. This could be explained by the different atomic size or mass between P and As which are more distinguishing parameters when bias is applied.

In all conditions, it can be concluded that several phenomena act on GF. First of all, there is the general level of resistivity: in case of low doping and high resistivity, the GF is higher. The Fc acts mainly on the resistivity but in this way, by decreasing resistivity it also decreases the GF.

The most key factors seem to be finally the dopant concentration and its nature. The effects involved by P or As are a bit different. According to the dopant concentration, the doping efficiency is not similar and the distribution of dopant between mono-crystalline grains and boundaries amorphous part changes. It seems, according to our model, that some of non-active dopant in terms of conductivity could negatively affect the piezoresitivity effect by creating traps inside the grain boundary or at the interface. These observations could be associated with the study of Rc/Rsh ratio which presents some links with GF at low Rc (<200 Ohm), this parameters could in a way quantify this trap level. That's the reason why some ICP modes such as the 900W pulsed mode or RF pulsed mode by curing this interface and decreasing the trap level lead to an increase in GF.

5. Conclusions

This article investigated low temperature µ-Si layers from ICP-CVD for strain gauge applications. Using the background available with the low temperature µ-Si PECVD, it was decided to dilute SiH_4 in a H_2/Ar mixture. All processes and optimization have been performed to fit with plastic and flexible electronics by limiting the thermal stress below 200°C. We first describe the ICP-CVD facilities used for the studies and especially the interest to use an H_2/Ar mixture to enhance the Fc of µ-Si layers as previously shown in PECVD. The positive impact of Ar dilution in ICP-CVD process was shown by improving widely resistivity of As doped µ-Si layers. We mention the Raman spectroscopy used to define the Fc and we also describe the bending test bench used to extract the GF. It consists of TLM structures under stress on different radii cylinders. Each radius corresponds to a % of the applied strain which produces resistance shift. From these measurements it could be extracted the resistivity, sheet resistance (Rsh), the contact resistance Rc and also GF.

The experiments exposed in this paper study the effects of different parameters such as the nature of dopant and its concentration in the plasma, the adjunction of RF power (bias voltage) to the ICP power in continuous or pulsed mode and finally the interest of high ICP power pulses during the deposition process of µ-Si layers.

Results show the general relationship between resistivity and GF which coherent for this level of doping. Under a certain value of Rc (<200 Ohm) a relationship between GF and Rc/Rsh ratio appears. They also show the non-systematic relationship between Fc and GF. But they also highlight some effects of the dopant concentration and especially its nature. According to the final strain gauge application, it might be necessary to give preference to GF or either to low resistivity in the case of a dynamic sensor for example.

To explain those results, a simple model has been introduced, explaining that the non-active dopants are located in the amorphous part of the layer (grain boundaries) and act negatively on the GF as a density of traps. The various ICP modes act either on the dopant incorporation inside monocrystalline grain or either on the density level of these traps.

In next experiments, we will further investigated P-type strain gauges and the concentration of dopant flow will be studied more exhaustively in order to define more precisely the right window to carry out a high GF layer with ICP-CVD associated with low resistivity for dynamic strain gauges applications.

6. Acknowledgments

The optimization of µ-Si layers, TLM tests and device fabrication has been performed on the NanoRennes platform with the support of CNRS French national research agency and the CPER Sophie/STIC&Ondes project.

7. References

[1] T. Someya, Y. Kato, T. Sekitani, S. Iba, Y. Noguchi, Y. Murase, H. Kawaguchi, T. Sakurai, "Conformable, flexible, large-area networks of pressure and thermal sensors with organic transistor active matrixes", Proc. Nat. Acad. Sci. 102 (35) (2005) 12321-12325

[2] S. Jung, T. Ji, V.K. Varadan, "Point of care temperature and respiration monitoring sensors for smart fabric applications", Smart Mater. Struct. 15 (2006) 1872-1876

[3] D.H. Kim, N. Lu, R. Ma, Y.S. Kim, R.H.Kim, S. Wang, J. Wu, S.M.Won, H. Tao, A.Islam, K.J. Yu, T. Kim, R. Chowdhury, M. Ying, L. Xu, M. Li, H.J. Chung, H. Keum, M. McCormick, P. Liu, Y.W. Zhang, F.G. Omenetto, Y. Huang, T. Coleman, J.A. Rogers, "Epidermal electronics", Science 333 (6044) (2011) 838-843

[4] R.B. Katragadda, Y. Xu, "A novel intelligent textile technology based on silicon flexible skins", Sens. Actuators A 143 (2007) 169-174

[5] E. Fallettaa, P. Costab, C. Della Pinaa, S. Lanceros-Mendez, "Development of high sensitive polyaniline based piezoresistive films by conventional and green chemistry approaches", Sens. Actuators A 220 (2014) 13–21

[6] A. Bessonova, M. Kirikovaa, S. Haqueb, I. Gartseeva, M.J.A. Bailey, "Highly reproducible printable graphite strain gauges for flexible devices", Sens. Actuators A 206 (2014) 75–80

[7] D. Lee, H.P. Hong, M.J. Lee, C.W. Park, N.K. Min, "A prototype high sensitivity load cell using single walled carbon nanotube strain gauges", Sens. Actuators A 180 (2012) 120–126

[8] N. Lu, C. Lu, S. Yang, J. Rogers, "Highly Sensitive Skin-Mountable Strain Gauges Based Entirely on Elastomers", Adv. Funct. Mater. 22 (19) (2012) 4044-4050

[9] S. Yang, N. Lu, "Gauge factor and stretchability of silicon-on-polymer strain gauges", Sensors 13 (7) (2013) 8577-8594

[10] L. Zhou, S. Jung, E. Brandon, and T. N. Jackson, "Flexible substratemicro-crystalline silicon and gated amorphous silicon strain sensors,"IEEE Trans. Electron Devices, 53, (2), (2006). 380–385.

[11] P.J. French, A.G.R. Evans, "Piezoresistance in polysilicon and its applications to strain gauges", Solid State Electron. 32 (1) (1989) 1-10

[12] H. Gleskova, S. Wagner, W. Soboyejo, Z. Suo, "Electrical response of amorphous silicon thin-film transistors under mechanical strain", J. Appl. Phys. 92 (2002) 6224-6229

[13] P. J. French, "Polysilicon: a versatile material for microsystems," Sensors and Actuators a-Physical, 99, (2002),

3-12.

[14] A. Matsuda (1999), “Growth mechanism of microcrystalline silicon obtained from reactive plasmas”, Thin Solid Films 337 (1-2)(1999) 1-6

[15] S. Hamma, P. Roca i Cabarrocas, “Low temperature growth of highly crystallized silicon thin films using hydrogen and argon dilution”, J. Non-Cryst. Solids 227–230 (2) (1998) 852-856

[16] P. Roca i Cabarrocas, “Plasma enhanced chemical vapor deposition of amorphous, polymorphous and microcrystalline silicon films,” J. Non-Cryst. Solids, 266–269 (2000) 31–37

[17] K. Kandoussi, C. Simon, N. Coulon, K. Belarbi, and T. Mohammed-Brahim, “Nanocrystalline silicon TFT process using silane diluted in argon–hydrogen mixtures”, J. Non-Cryst. Solids 354 (19) (2008) 2513–2518

[18] Y. Kervran, O. De Sagazan, S. Crand, N. Coulon, T. Mohammed-Brahim, O. Brel, “Microcrystalline silicon: strain gauge and sensor arrays on flexible substrate for the measurement of high deformations”, Sens. Actuators A: Phys. 236 (2015) 273-280

[19] H. P. Zhou, D.Y. Wei, S. Xu, S.Q. Xiao, L.X. Xu, S.Y. Huang, Y. N. Guo, S. Khan, M. Xu, “Crystalline silicon surface passivation by intrinsic silicon thin films deposited by low-frequency inductively coupled plasma,, J. Appl. Phys. 112 (1) (2012) 013708

[20] M. Goto, H. Toyoda, M. Kitagawa, T. Hirao, H. Sugai, “Low Temperature Growth of Amorphous and Polycrystalline Silicon Films from a Modified Inductively Coupled Plasma”, Jpn. J. Appl. Phys. 36(6A) (1997) 3714

[21] C.-H. Shen,J.M. Shieh, J.Y. Huang, H.-C. Kuo, C.-W. Hsu, B.-T. Dai, C.-T. Lee, C.L. Pan, F.L. Yang, “Inductively coupled plasma grown semiconductor films for low cost solar cells with improved light-soaking stability”, Appl. Phys. Lett. 99 (3) (2011) 033510-3

[22] S. Q. Xiao, S. Xu, H.P. Zhou, D.Y. Wei, S.Y. Huang, L.X. Xu, C.C. Sern, Y.N. Guo, S. Khan , “Amorphous/crystalline silicon heterojunction solar cells via remote inductively coupled plasma processing”, Appl. Phys. Lett. 100 (23) (2012) 233902

[23] Q. Cheng, S. Xu, J. Long, S. Huang, and J. Guo, “Homogeneous nanocrystalline cubic silicon carbide films prepared by inductively coupled plasma chemical vapor deposition”, Nanotechnology 18 (46) (2007) 465601

[24] T. Frischmuth, M. Schneider, D. Maurer, T. Grille, and U. Schmid, “Inductively-coupled plasma-enhanced chemical vapour deposition of hydrogenated amorphous silicon carbide thin films for MEMS”, Sens. Actuators Phys. 247 (2016) 647–655

[25] C. Jeong, Y.B. Kim,S.-H Lee, J.H. Kim, “Preparation of Born-Doped a-SiC:H Thin Films by ICP-CVD Method and to the Application of Large-Area Heterojunction Solar Cells”,Journal of Nanoscience and Nanotechnology 10 (5) (2010) 3321-3325

[26] C.H. Jeong, M.S. Jeon, K. Koichi, “Electrical Properties of Boron and Phosphorus Doped μc-Si: H Films using Inductively Coupled Plasma Chemical Vapor Deposition Method for Solar Cell ApplicationsTransactions on Electrical, 2008 - koreascience.or.kr

[27] G. Nogay, E. Özkol, S. Ilday, and R. Turan, “Structural peculiarities and aging effect in hydrogenated a-Si prepared by inductively coupled plasma assisted chemical vapor deposition technique”, Vacuum 110 (2014) 114–120

[28] D. J. Gardiner and P. R. Graves, Eds., “Practical Raman Spectroscopy”,. Berlin Heidelberg: Springer-Verlag, 1989

[29] H. Wernerus, M. Bivour, L. Kroely, M. Hermle, and W. Wolke, “Characterization of Ultra-thin μc-Si:H Films for Silicon Heterojunction Solar Cells”, Energy Procedia 55 (2014) 310–319

[30] G. Viera, S. Huet, and L. Boufendi, “Crystal size and temperature measurements in nanostructured silicon using Raman spectroscopy”, J. Appl. Phys. 90 (2001) 4175–4183

[31] J. Zi, H. Büscher, C. Falter, W. Ludwig, K. Zhang, and X. Xie, “Raman shifts in Si nanocrystals”, Appl. Phys. Lett. 69 (2) (1996) 200–202

[32] E. Anastassakis, “Strain characterization of polycrystalline diamond and silicon systems”, J. Appl. Phys. (86) (1999) 249–258

[33] S. Grover, “Effect of Transmission Line Measurement (TLM) Geometry on Specific Contact Resistivity Determination”, thesis Rochester Institute of Technology, 2016

[34] P. Alpuim, V. Correia, E.S. Martins, J.G. Rocha, I.G. Trindade, S. Lanceros-Mendez, “Piezoresistive silicon thin film sensor array for biomedical applications”, Thin Solid Films 519 (2011) 4574–4577

[35] H. Gleskova, S. Wagner, Z. Suo, “Failure resistance of amorphous silicon transistors under extreme in-plane strain”, Appl. Phys. Lett. 75 (1999) 3011-3013

[36] Technical Data sheet, DuPont Kapton HN (available online)

[37] J. Gaspar, A. Gualdino, B. Lemke, O. Paul, V. Chu, J.P. Conde, “Mechanical and piezoresistive properties of thin silicon films deposited by plasma-enhanced chemical vapor deposition and hot-wire chemical vapor deposition at low substrate temperatures”, J. Appl. Phys. 112 (2) (2012) 024906-14

[38] H. Dong, Y. Kervran, N. Coulon, O. de Sagazan, E. Jacques, T. Mohammed-Brahim, “Highly flexible microcrystalline silicon n-type TFT on PEN bent to a curvature radius of 0.75 mm”, IEEE Transactions on Electron Devices 62 (10) (2015) 3278-3284

[39] P. Alpuim, J. Gaspar, P. Gieschke, C. Ehling, J. Kistner, N.J. Goncalves, M.I. Vasilevskiy, O. Paul, “Study of the piezoresistivity of doped nanocrystalline silicon thin films”, J. Appl. Phys. 109 (2011) 123717

[40] P. Alpuim, S.A. Filonovich, C.M. Costa, P.F. Rocha, M.I. Vasilevskiy, S. Lanceros-Mendez, C. Fria, A. Torres Marques, S. Roares, C. Costa, “Fabrication of a strain sensor for bone implant failure detection based on piezoresistive doped nanocrystalline silicon”, J. Non-Cryst. Sol. 354 (2008) 2585–2589

[41] J.F.Bresse, S.Blayac, “ Epitaxial layer sheet resistance outside and under ohmic contacts measurements using electrostatic force microscopy”, Solid-State Electronics 45 (7), (2001) 1071-1076